JACS
JOURNAL OF THE AMERICAN CHEMICAL SOCIETY
Article
pubs.acs.org/JACS

Autocatalytic Fluorescence Photoactivation

Ek Raj Thapaliya, Subramani Swaminathan, Burjor Captain, and Françisco M. Raymo*

Laboratory for Molecular Photonics, Department of Chemistry, University of Miami, 1301 Memorial Drive, Coral Gables, Florida 33146-0431, United States

Supporting Information

ABSTRACT: We designed an autocatalytic photochemical reaction based on the photoinduced cleavage of an α-diketone bridge from the central phenylene ring of a fluorescent anthracene derivative. The product of this photochemical transformation sensitizes its own formation from the reactant, under illumination at a wavelength capable of exciting both species. Specifically, the initial and direct excitation of the reactant generates the product in the ground state. The subsequent excitation of the latter species results in the transfer of energy to another molecule of the former to establish an autocatalytic loop. Comparison of the behavior of this photoactivatable fluorophore with that of a model system and the influence of dilution on the reaction progress demonstrates that the spectral overlap between the emission of the product and the absorption of the reactant together with their physical separation govern autocatalysis. Indeed, both parameters control the efficiency of the resonant transfer of energy that is responsible for establishing the autocatalytic loop. Furthermore, the proximity of silver nanoparticles to reactant and product increases the energy-transfer efficiency with a concomitant acceleration of the autocatalytic process. Thus, this particular mechanism to establish sensitization offers the opportunity to exploit the plasmonic effects associated with metallic nanostructures to boost photochemical autocatalysis.

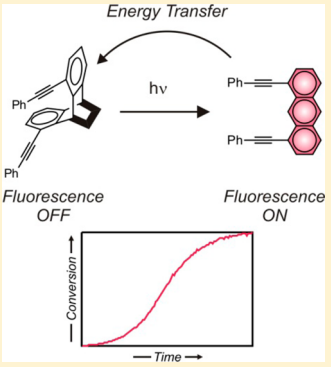

INTRODUCTION

Replicating molecules catalyze their own formation from appropriate precursors.[1] In most instances, supramolecular contacts between product and reactants template the assembly of an identical copy of the former from the latter species. Under these conditions, the reaction rate increases, during the course of the chemical transformation, to impose a sigmoidal temporal dependence on the concentration of the replicating product.[2] Such a kinetic amplification is responsible for a diversity of biochemical processes and is believed to have played a fundamental role in the origin of life.[3] In fact, a number of artificial counterparts to replicating biomolecules have been developed already with the ultimate goal of elucidating the basic factors responsible for autocatalysis.[1] Photochemical analogues of supramolecular replicators remain, instead, limited to a few remarkable examples, mostly aimed at signaling molecular recognition with changes in fluorescence intensity.[4−10] Indeed, the unique kinetic profile of autocatalytic reactions can be exploited to impose the amplification on fluorescence signaling that is particularly convenient for chemical sensing.[11]

Photoactivatable fluorophores switch from a nonemissive to an emissive state under irradiation at an appropriate activation wavelength (λ_{Ac}).[12] Illumination of the resulting product at a given excitation wavelength (λ_{Ex}) then produces significant fluorescence. The concatenation of a photochemical reaction (activation) with a photophysical process (fluorescence) is therefore responsible for the operating principles of these photoresponsive compounds. Their unique behavior, in combination with the interplay of beams illuminating at λ_{Ac} and λ_{Ex}, can be exploited to switch fluorescence on within a defined region of space at a particular interval of time. In turn, such a spatiotemporal control permits the monitoring of dynamic events in real time[13] and the visualization of samples with subdiffraction resolution.[14] Indeed, photoactivatable fluorophores are becoming invaluable probes for the investigation of the dynamic and structural properties of a diversity of specimens.

In the wake of our research efforts directed at the identification of viable structural designs to photoactivate fluorescence,[12−14] we realized that the photochemical and photophysical events responsible for switching emission on can be manipulated to engineer an autocatalytic transformation. Specifically, the structures of the nonemissive reactant and fluorescent product can be selected to permit excitation of both at the same wavelength ($\lambda_{Ac} = \lambda_{Ex}$) as well as to ensure a significant overlap between the absorption spectrum of the former and the emission spectrum of the latter. Under these conditions, irradiation would excite the reactant to generate the product first and then excite the product to sensitize the excitation of another reactant, establishing an autocatalytic loop. Indeed, either the resonant transfer of the excitation energy of the product to a proximal reactant or the reabsorption of its fluorescence by a distal reactant would translate into sensitization. These operating principles are reminiscent of the energy cascades governing quantum amplification in certain photochemical processes.[15−20] In such chain reactions, the excitation of the reactant eventually generates the product in an excited state. The resulting species can then transfer energy to another reactant molecule, ensuring

Received: July 7, 2014
Published: September 10, 2014

   dx.doi.org/10.1021/ja5068383 | J. Am. Chem. Soc. 2014, 136, 13798−13804

the propagation of the chain reaction, and decay to the ground state. The overall result is that the absorption of a single photon by the reactant can produce multiple copies of the product, leading to quantum amplification. In these processes, however, the product sensitizes its own formation prior to populating its ground state, and therefore, the concentration of its ground state has no influence on the rate of the overall transformation. According to our design logic, instead, the product is formed in the ground state first and then it is excited directly to sensitize its own formation. Thus, while the absorption of multiple photons is still required to form multiple copies of the product, the increasing concentration of the latter in the ground state, during the course of the reaction, can accelerate the photochemical conversion and lead to autocatalysis. Furthermore, such a mechanism for the realization of a photochemical replicator could be accelerated even further with the aid of plasmonic effects.[21] In fact, the enhancement of the electromagnetic field in close proximity to the surface of illuminated metallic nanostructures can increase the efficiencies of photochemical reactions[22] and photophysical processes.[23] Therefore, the conversion of reactant into product and the emission of the latter could both be promoted with metallic nanostructures to boost the overall autocatalytic process.

The introduction of an α-diketone bridge across positions 9 and 10 of anthracene isolates electronically the two peripheral phenylene rings of the oligoacene platform.[24] The absorption spectrum of the resulting adduct shows a broad and weak band in the visible region for a $n \rightarrow \pi^*$ transition of the α-diketone chromophore.[25] Illumination at wavelengths within this band results in the cleavage of the α-diketone bridge with the release of two molecules of carbon monoxide and the regeneration of anthracene.[26] In fact, the photoinduced cleavage of similar α-diketone adducts has been employed already to prepare photochemically several oligoacenes[27] and, in a few instances, to activate fluorescence.[28,29] Furthermore, these photochemical reactions can be performed efficiently within rigid matrices to avoid the dimerization and oxidation of the resulting oligoacenes that often accompany these transformations in solution and, hence, permit the isolation of otherwise elusive polycyclic aromatic hydrocarbons.[30,31] These literature precedents suggest that an anthracene derivative, capable of emitting in the same spectral region where the α-diketone bridge absorbs, should sensitize its own formation from the corresponding adduct upon excitation. On the basis of such considerations, we designed an α-diketone adduct able to satisfy these stringent spectral requirements as well as identified a control system with minimal spectral overlap instead. In this article, we report the synthesis of the former compound, the structural characterization of both adducts together with the investigation of their photochemical and photophysical properties and the influence of silver nanoparticles on the behavior of the former species.

RESULTS AND DISCUSSION

Design, Synthesis and Structural Characterization. Adducts **1** and **2** differ in the nature of the group (R in Figure 1) on their two *ortho*-phenylene rings and, upon illumination, are supposed to generate **3** and **4** respectively. This particular group is expected to have a negligible influence on the $n \rightarrow \pi^*$ absorption of the α-diketone bridge of **1** and **2**, but a pronounced effect on the emission of **3** and **4** and, hence, on the spectral overlap between reactant and product of the two photochemical reactions.

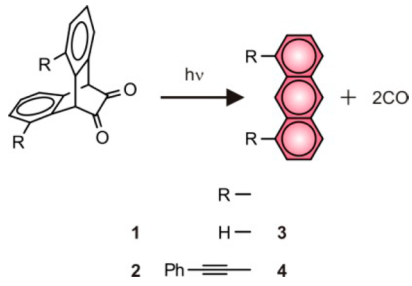

Figure 1. Photoinduced decarbonylation of **1** and **2** to produce **3** and **4**, respectively.

Adduct **1** can be prepared from **3** in three synthetic steps, following a literature protocol.[32] The very same protocol can be adapted to convert **4** into **2** (Figure 2). Specifically, treatment of **4** with vinylene carbonate results in the bridging of positions 9 and 10 of the anthracene core with the formation of **5**. Basic hydrolysis of **5** and then oxidation of **6** convert the corresponding bridging unit into a photocleavable α-diketone in the shape of **2**. The overall yield for the three consecutive synthetic steps is 26%.

The structural identities of **2**, **5** and **6** were confirmed by electrospray ionization mass spectrometry (ESIMS) together with ^{1}H and ^{13}C nuclear magnetic resonance (NMR) spectroscopies (Figures S1−S3, Supporting Information (SI)). In addition, single crystals of **1** and **2** suitable for X-ray diffraction analysis (Table S1 (SI)) were obtained after diffusion of hexane vapors into benzene solutions of the compounds. The resulting structures (Figure 3) clearly reveal that the α-diketone bridge, between positions 9 and 10, forces the three fused rings out of planarity and interrupts electronic conjugation across them.

Photochemical and Photophysical Properties. The absorption spectra of **1** and **2** (***a*** and ***b*** in Figure 4) reveal a broad and weak band centered at 462 nm (λ_{Ab} in Table 1) for a $n \rightarrow \pi^*$ transition of the α-diketone bridge. Upon visible illumination, the characteristic vibronic structure of the corresponding anthracene chromophores appear between 300 and 450 nm (Figure 4c,d). These absorptions are identical to those observed in the spectra of **3** and **4** (Figure S4a,b (SI)) and demonstrate that the α-diketone bridge of **1** and **2** cleaves under irradiation to restore the anthracene chromophore, in agreement with literature precedents.[24−31] Similar changes are also evident in the corresponding emission spectra (e → g and f → h in Figure 4). Intense bands appear between 350 and 600 nm (λ_{Em} in Table 1) only after visible illumination of the sample. Once again, the photogenerated bands are identical to those observed in the spectra of **3** and **4** (Figure S4c,d (SI)). Thus, the photoinduced conversion of nonemissive reactants **1** and **2** into emissive products **3** and **4**, respectively, translates into efficient fluorescence activation.

The photoinduced conversion of **1** and **2** into **3** and **4** respectively occurs in poly(butyl methacrylate) (PBMA) matrix as well as in acetonitrile solution with essentially identical spectral changes (Figures 4 and S5 (SI)). The polymer matrix, however, is relatively rigid and prevents the diffusion of the entrapped species. Fluorescence images (Figure S6a,b (SI)) of a polymer film doped with **2** reveal significant emission only after visible illumination. Specifically, the irradiation of a circular area at the center of the imaging field with a laser operating at 458 nm switches **2** to **4** exclusively in the illuminated area with the concomitant appearance of intense fluorescence. The very same

dx.doi.org/10.1021/ja5068383 | J. Am. Chem. Soc. 2014, 136, 13798−13804

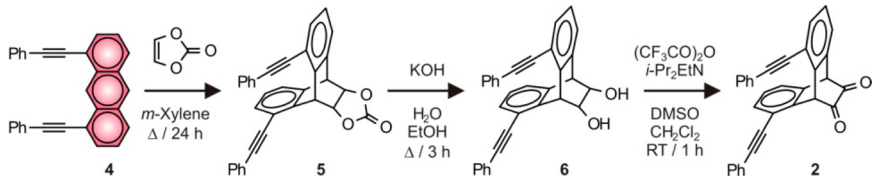

Figure 2. Three-step synthesis of **2** from **4**.

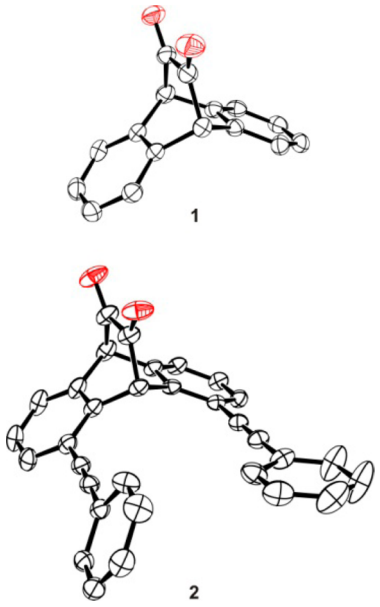

Figure 3. ORTEP representations of the crystal structures of **1** and **2** (30 and 50% thermal ellipsoid probability, respectively).

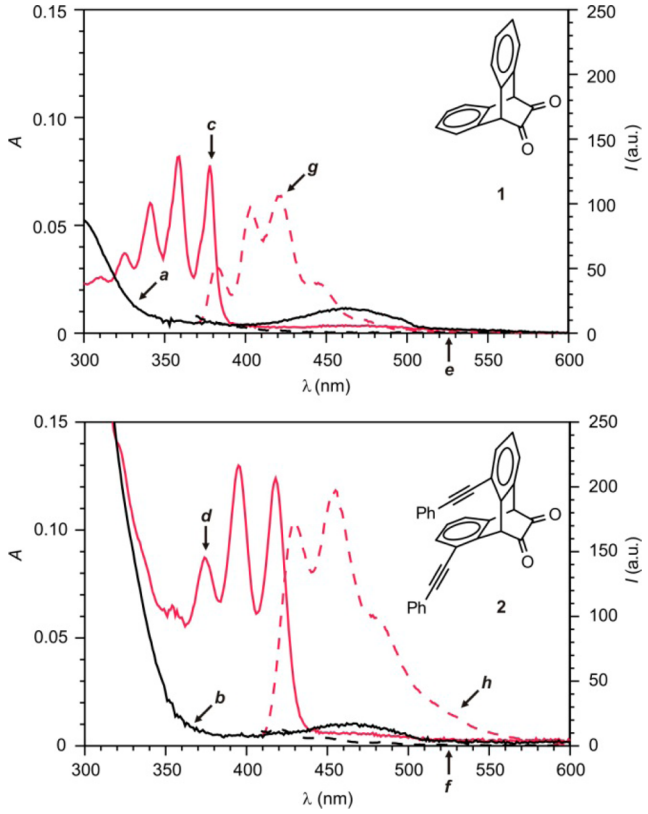

Figure 4. Absorption (a–d) and emission (e–h) spectra of PBMA films, doped (8% w/w) with **1** (λ_{Ex} = 350 nm) or **2** (λ_{Ex} = 390 nm) and spin coated on quartz slides, before (a, b, e and f) and after (c, d, g and h) irradiation (420 nm, 2.3 mW cm^{-2}, 300 s for **1** and 60 s for **2**).

fluorescent spot is also evident in an image (Figure S6c (SI)) recorded after as many as 10 min, confirming the lack of any significant diffusion.

The inability of reactant and product to diffuse within the polymer matrix offers the opportunity to induce and probe the transformation of one into the other in a portion of the film with the sole aid of the excitation source of an emission spectrometer. In particular, the sequential acquisition of emission spectra (Figure 5) of a PBMA film doped with **2** shows the gradual growth of the characteristic bands of **4**. These spectra were recorded under excitation at a wavelength (390 nm) that matches the 0 → 2 absorption band (Figure 4d) of the photogenerated anthracene chromophore. At this wavelength, the absorbance of **2** (Figure 4b) is relatively small, yet it is sufficient to initiate the photochemical generation of **4**. Once formed, **4** can absorb part of the incoming photons and emit as a result. In turn, its emission can induce the conversion of another molecule of **2** into a new molecule of **4** and establish an autocatalytic loop. Indeed, a plot (Figure 6a) of the emission intensity, detected at 453 nm in the sequence of spectra, shows the sigmoidal temporal dependence typical of autocatalysis.[2] The reaction accelerates significantly with an increase in the product concentration. By contrast, the same experiment performed with **1** does not reveal any change in fluorescence over the same temporal scale (Figure 6b).[33] Indeed, comparison of the emission spectra of **3** and **4** (Figure 4g,h) reveals optimal spectral overlap with the α-diketone absorption of the corresponding adduct (Figure 4a,b) only for the latter. In particular, the overlap integral (J in Table 1) for the **2**/**4** pair is 22.4 × 10^{-16} M^{-1} cm^{-1}, while it is only 8.3 × 10^{-16} M^{-1} cm^{-1} for the **1**/**3** counterpart. These values correspond to Förster distances (R_0 in Table 1) of 26 and 18 Å respectively and energy-transfer efficiencies (E in Table 1) of 25.8 and 0.3% respectively at a dopant concentration of 8% w/w relative to the polymer.[34] Thus, only one of the two photochemical products can transfer efficiently its excitation energy to the corresponding reactant and sensitize its own formation in full agreement with the pronounced difference between the photokinetic profiles of the two reactions (Figure 6a,b).[35]

The role of resonant energy transfer in imposing the sigmoidal profile on the photoinduced conversion of **2** into **4** is further confirmed by the effect of dilution on the reaction course.[36] Specifically, a 10-fold dilution of the sample increases the time required to convert 50% of the reactant from 1450 to 3200 s (Figure 7a,b). Indeed, the average distance between molecules elongates sufficiently with dilution to lower the energy-transfer efficiency to only 0.01%. Consistently, fittings (Figures S7 and S8 (SI)) of the corresponding sigmoidal plots indicate a 35-fold decrease in the quantum yield for the

dx.doi.org/10.1021/ja5068383 | J. Am. Chem. Soc. 2014, 136, 13798–13804

Table 1. Photochemical and Photophysical Parameters

	λ_{Ab}[a] (nm)	λ_{Em}[a] (nm)	ϕ_A[b]	ϕ_F[c]	J[d] (10^{-16} M^{-1} cm^3)	R_0[d] (Å)	E[e] (%)
1 → **3**	462	381, 403, 421, 445	0.20	0.27	8.3	18	0.3
2 → **4**	462	430, 454, 479	0.51	0.85	22.4	26	25.8

[a]Wavelengths at the absorption (λ_{Ab}) and emission (λ_{Em}) maxima of reactant and product, respectively, in PBMA at 25 °C. [b]The activation quantum yield (ϕ_A) is the quantum yield for the photochemical conversion of reactant into product. This parameter was determined by illuminating aerated MeCN solutions of the reactant within the chamber of a photoreactor (420 nm) and monitoring periodically the formation of the product by absorption spectroscopy. The irradiation power per unit area (2.3 mW cm^{-2}) was measured with a potassium ferrioxalate actinometer, and this value was used to estimate ϕ_A from the corresponding absorbance evolution during photolysis, according to an established procedure (ref 41). The error in the determination of ϕ_A is ca. 15%. [c]Literature values for the fluorescence quantum yield (ϕ_F) of the product in aerated MeCN at 25 °C (ref 40). [d]Overlap integral (J) and Förster distance (R_0) estimated from the spectra recorded in aerated MeCN at 25 °C. [e]Efficiency (E) of energy transfer from product to reactant estimated from the value of R_0 and the average distance between molecules in PBMA at a concentration of 8% w/w relative to the polymer.

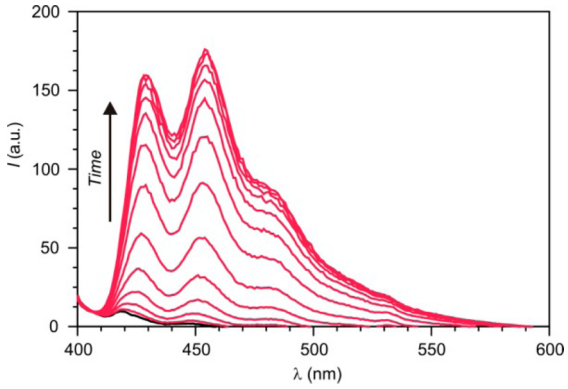

Figure 5. Emission spectra (λ_{Ex} = 390 nm) of a PBMA film, doped with **2** (8% w/w) and spin coated on a quartz slide, recorded consecutively over the course of 3000 s (scan rate = 10 nm s^{-1}) at 25 °C.

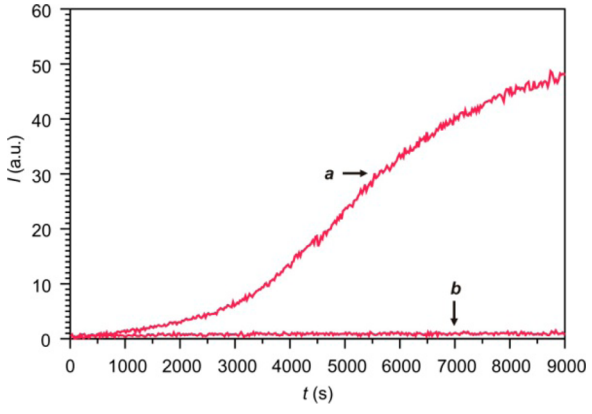

Figure 6. Evolution of the emission intensity (λ_{Ex} = 350 nm) of PBMA films, doped (8% w/w) with **2** (a, λ_{Em} = 453 nm) or **1** (b, λ_{Em} = 400 nm) and spin coated on quartz slides, during the sequential acquisition of spectra over the course of 9000 s (scan rate = 10 nm s^{-1}) at 25 °C.

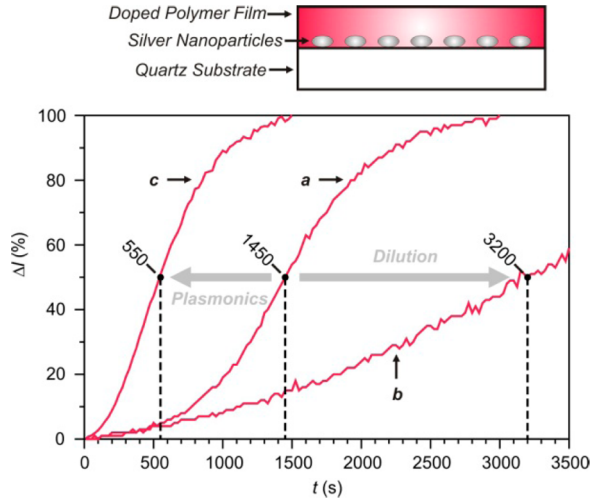

Figure 7. Evolution of the emission intensity (λ_{Ex} = 390 nm, λ_{Em} = 453 nm) of PBMA films, doped with **2** at a concentration of 8 (a) or 0.8% w/w (b), relative to the polymer, in the absence of silver nanoparticles or at a concentration of 8% w/w (c) in their presence and spin coated on quartz slides, during the sequential acquisition of spectra over the course of 3000 s (scan rate = 10 nm s^{-1}) at 25 °C.

sensitized formation of **4**, under illumination at 390 nm, with dilution.[37]

In these experiments, the irradiation wavelength of 390 nm is essentially both λ_{Ac} as well as λ_{Ex}. The initial activation of the reactant and the subsequent excitation of the product are both a consequence of absorption at this particular wavelength, which happens to fall within the spectral range associated with the surface-plasmon band of silver nanoparticles (Figure S10 (SI)).[38] As a result of the local enhancement in electromagnetic field,[21−23] these metallic nanostructures can therefore promote the transformation of **2** into **4** in their proximity, under such illumination conditions. Indeed, the sequential acquisition of emission spectra (Figure S11 (SI)) of a PBMA film, doped with **2** and spin coated on silver nanoparticles deposited on a quartz slide, reveals the developing bands of **4** with, yet again, a sigmoidal temporal dependence (Figure 7c) of the emission intensity. However, the time required to convert 50% of the reactant is only 550 s in the presence of the silver nanoparticles, while it is 1450 s in their absence. Fittings (Figures S8 and S9 (SI)) of the corresponding sigmoidal plots indicate a 1.6-fold increase in the quantum yield for the sensitized formation of **4** under the influence of the metallic nanostructures.[37]

The effect of the nanoparticles on the photoinduced conversion of **2** into **4** can be a result of their ability to facilitate the direct excitation of the reactant and the conversion of the resulting excited state into the product. Alternatively, the nanostructures can promote the excitation of the product, enhance its emission and, hence, encourage sensitization. Comparison of the emission spectra (Figure S12a,b (SI)) of **4**, recorded without and with silver nanoparticles, suggests that the latter mechanism is mostly responsible for accelerating the autocatalytic process. Indeed, the fluorescence of **4** increases significantly in the presence of the nanoparticles. Specifically, the ratio between the integrated emission intensities measured with the nanoparticles and that recorded without is 2.7. Such an enhancement in the fluorescence of **4** elongates the Förster distance to 31 Å and increases the energy transfer to 48%. Interestingly, the ratio between the energy transfer efficiencies, estimated with and without the silver nanoparticles, is 1.8. This

dx.doi.org/10.1021/ja5068383 | J. Am. Chem. Soc. 2014, 136, 13798−13804

value is remarkably close to the enhancement (cf. 1.6) in photoactivation efficiency determined from the sigmoidal plots. Thus, the role of the metallic nanostructures in accelerating the autocatalytic conversion of **2** into **4** appears to be predominantly a consequence of their ability to promote energy transfer from the product to the reactant.

CONCLUSIONS

Photochemical autocatalysis can be implemented on the basis of fluorescence activation. The fluorescent product of such a photochemical transformation must be designed to emit in the same range of wavelengths where the nonemissive reactant absorbs. If both species can be excited at the same wavelength and if they are maintained in close proximity, then resonant energy transfer from the product to the reactant can sensitize the formation of the latter from the former to establish an autocatalytic loop. Furthermore, the local enhancement in electromagnetic field, associated with the illumination of metallic nanoparticles, can be exploited to enhance the energy-transfer efficiency and accelerate the overall photochemical transformation. Ultimately, such operating principles for autocatalysis with plasmonic boost translate into fluorescence amplification. Thus, our representative example of photochemical autocatalysis might eventually evolve into a general design logic for the realization of plasmonic systems capable of signal amplification.

EXPERIMENTAL SECTION

Materials and Methods. Chemicals were purchased from commercial sources and used as received with the exception of CH_2Cl_2 and MeCN, which were distilled over CaH_2, and H_2O, which was purified with a Barnstead International NANOpure Diamond Analytical system. Compounds **1** and **4** were prepared according to literature procedures.[32,39] EISMS was performed with a Bruker micrOTO-Q II spectrometer. NMR spectra were recorded with a Bruker Avance 400 spectrometer. Absorption and emission spectra were recorded with Varian Cary 100 Bio and Varian Cary Eclipse spectrometers, respectively. Measurements were performed either in aerated MeCN solutions, using quartz cells with a path length of 1.0 cm, or in PBMA matrices, using quartz slides mounted on custom-built sample holders. The values of ϕ_F listed in Table 1 are literature data.[40] Those of ϕ_A listed in the same table are the quantum yields for the photochemical conversions of **1** into **3** and of **2** into **4** in aerated acetonitrile at 25 °C. The values of ϕ_A were determined by monitoring the evolving absorbance of the photochemical product under illumination at 420 nm, using a potassium ferrioxalate actinometer to measure the irradiation power per unit area (2.3 mW cm^{-2}) with an established procedure.[41] Samples were illuminated with a Luzchem Research LZC-4V photoreactor (420 nm, 2.3 mW cm^{-2}) for the experiments in Figures 4 and S5 (SI) and with the excitation source (350 or 390 nm) of the emission spectrometer for the experiments in Figures 6, 7, and S7. A Chemat Technologies KW-4A spin coater was used to prepare the polymer films. A Tencor Instruments 10−00090 surface profilometer was used to measure the thickness of the polymer films. Fluorescence images were recorded with a Leica SP5 confocal laser-scanning microscope.

2. Trifluoroacetic anhydride (1 mL, 7.0 mmol) was added dropwise over 10 min to a mixture of dry DMSO (1 mL) and CH_2Cl_2 (4 mL) maintained at −60 °C under Ar. The resulting solution was stirred under these conditions for a further 10 min and then a solution of **6** (180 mg, 0.4 mmol) in a mixture of dry DMSO (1 mL) and dry CH_2Cl_2 (2 mL) was added dropwise over 10 min. The resulting solution was stirred for a further 60 min under the same conditions and then *i*-Pr_2EtN (2.7 mL, 16 mmol) was added dropwise over 5 min. The resulting solution was stirred for a further 60 min and then it was allowed to warm up to ambient temperature. After dilution with CH_2Cl_2 (50 mL), the mixture was washed with aqueous HCl (1 M, 20 mL), H_2O (20 mL) and brine (20 mL). The organic layer was dried over Na_2SO_4 and then the solvent was distilled off under reduced pressure. The residue was purified by column chromatography [SiO_2:AcOEt/hexanes (2:3, v/v)] to give **2** (90 mg, 50%) as a yellow solid: ESIMS m/z = 457.1202 $[M + Na]^+$ (m/z calcd. for $C_{32}H_{18}O_2Na$ =457.1204); ^1H NMR ($CDCl_3$) δ = 5.04 (1H, s), 6.22 (1H, s), 7.14−7.19 (4H, m), 7.29−7.34 (2H, m), 7.37−7.40 (2H, m), 7.43−7.48 (6H, m), 7.59−7.61 (2H, d, 8 Hz); ^{13}C NMR ($CDCl_3$) δ = 56.4, 60.4, 85.7, 95.0, 122.5, 122.7, 126.4, 128.8, 129.1, 129.6, 132.3, 133.1, 135.8, 136.3, 183.0, 184.0.

5. A solution of **4** (360 mg, 0.9 mmol) and vinylene carbonate (1 mL, 16 mmol) in *m*-xylene was heated at 180 °C in sealed tube for 24 h. The reaction mixture was cooled down to ambient temperature and diluted with dry MeOH (50 mL). The resulting precipitate was filtered off, washed with MeOH (100 mL) and dried to give **5** (345 mg, 78%) as a white solid: ESIMS m/z = 487.1294 $[M + Na]^+$ (m/z calcd. for $C_{33}H_{20}O_3Na$ = 487.1309); ^1H NMR [$(CD_3)_2CO$] δ = 5.05 (1H, s), 5.13−5.18 (1H, m), 5.21−5.26 (1H, m), 5.95 (1H, s), 7.21−7.30 (4H, m), 7.31−7.44 (4H, m), 7.46−7.59 (8H, m); ^{13}C NMR ($CDCl_3$) δ = 43.9, 48.5, 76.3, 76.4, 86.2, 86.5, 93.9, 94.3, 121.6, 122.5, 122.9, 123.3, 125.8, 127.0, 127.9, 128.0, 128.7, 128.8, 129.0, 131.7, 131.9, 132.2, 136.9, 137.8, 138.5, 138.9, 154.4.

6. A mixture of **5** (320 mg, 0.7 mmol) and KOH (160 mg, 3 mmol) in H_2O (2 mL) and EtOH (10 mL) was heated at 80 °C for 3 h. The hot reaction mixture was filtered and the solid residue was purified by column chromatography [SiO_2:AcOEt/hexanes (1:1, v/v)] to give **6** (200 mg, 66%) as a white solid: ESIMS m/z = 461.1504 $[M + Na]^+$ (m/z calcd. for $C_{32}H_{22}O_2Na$ =461.1517); ^1H NMR [$(CD_3)_2CO$] δ = 4.05 (2H, s), 4.16 (1H, s), 4.42 (1H, s), 4.54 (1H, s), 5.65 (1H, s), 7.16−7.30 (6H, m), 7.32−7.52 (10H, m); ^{13}C NMR [$(CD_3)_2CO$] δ = 47.7, 52.0, 59.6, 67.0, 67.3, 86.8, 87.5, 91.8, 92.3, 119.4, 121.0, 123.0, 123.4, 125.0, 125.8, 126.5, 126.7, 128.3, 128.5, 128.5, 129.4, 129.8, 131.5, 131.6, 140.3, 141.0, 141.5.

Crystallographic Analysis. The data crystals of **1** and **2** were glued onto the end of a thin glass fiber. X-ray intensity data were measured with a Bruker SMART APEX2 CCD-based diffractometer, using Mo Kα radiation (λ = 0.71073 Å).[42] The raw data frames were integrated with the SAINT+ program by using a narrow-frame integration algorithm. Corrections for Lorentz and polarization effects were also applied with SAINT+. An empirical absorption correction based on the multiple measurement of equivalent reflections was applied using the program SADABS. The structures were solved by a combination of direct methods and difference Fourier syntheses and refined by full-matrix least-squares on F^2 with the SHELXTL software package.[43] All non-hydrogen atoms were refined with anisotropic displacement parameters. Hydrogen atoms were placed in geometrically idealized positions and included as standard riding atoms during the least-squares refinements. Crystal data, data collection parameters and results of the analysis are listed in Table S1 (SI).

Yellow single crystals were obtained after diffusion of hexane vapors into benzene solutions of **1** and **2**. Compound **1** crystallized in the monoclinic crystal system. The systematic absences in the intensity data identified the unique space group $P2_1/c$. Compound **2** crystallized in the triclinic crystal system, and the space group $P\bar{1}$ was assumed and confirmed by the successful refinement of the structure. Two molecules are present in the asymmetric crystal unit.

Silver Nanoparticles. Aqueous NaOH (1.2 M, 0.1 mL) was added to aqueous $AgNO_3$ (0.22 g, 26 mL) under vigorous stirring. A dark-brown precipitate formed immediately. Aqueous NH_4OH (7.3 M, 1 mL) was added dropwise to dissolve the precipitate. The resulting clear solution was cooled down to 5 °C. Quartz slides were submerged in the cooled solution and aqueous D-glucose (0.35 g, 4 mL) was added. The mixture was stirred for 2 min at 5 °C, allowed to warm up to ambient temperature, heated to 40 °C and stirred for a further 10 min at this temperature. In the process, the yellow-green solution turned brown and a greenish coating deposited on the slides. The slides were removed from the solution, washed with H_2O, sonicated in H_2O for 1 min at ambient temperature, washed again with H_2O, dried in air for 2 h and coated with the polymer films.

Polymer Films. A solution of PBMA ($M_W = 337 \times 10^3$) and either **1** or **2** (0.8, 2 or 8% w/w relative to PBMA) was deposited dropwise on either a glass or a quartz slide. The substrate was spun at 1000 rpm for 20 s and then again at 1000 rpm for a further 60 s. The coated slides were stored under reduced pressure for 6 h prior to any imaging (glass) and spectroscopic (quartz) experiments. The same protocol was employed to deposit polymer films on quartz slides precoated with silver nanoparticles.

■ ASSOCIATED CONTENT

Ⓢ Supporting Information

^{1}H and ^{13}C NMR spectra of **2**, **5** and **6**; crystallographic data (CIF) for **1** and **2**; absorption and emission spectra of **1**−**4** in MeCN; fluorescence images of **2** in PBMA before and after activation; kinetic model and fittings of the sigmoidal plots; absorption and emission spectra of **2** and silver nanoparticles in PBMA; emission spectra of **4** with and without silver nanoparticles in PBMA. This material is available free of charge via the Internet at http://pubs.acs.org.

■ AUTHOR INFORMATION

Corresponding Author

fraymo@miami.edu

Notes

The authors declare no competing financial interest.

■ ACKNOWLEDGMENTS

The National Science Foundation (CAREER Award CHE-0237578, CHE-0749840 and CHE-1049860) is acknowledged for financial support.

■ REFERENCES

(1) Bissette, A. J.; Fletcher, S. P. *Angew. Chem., Int. Ed.* **2013**, *52*, 12800−12826.

(2) von Kiedrowski, G. *Bioorg. Chem. Front.* **1993**, *3*, 113−146.

(3) Ruiz-Mirazo, K.; Briones, C.; de la Escosura, A. *Chem. Rev.* **2014**, *114*, 285−366.

(4) Hong, J. I.; Feng, Q.; Rotello, V.; Rebek, J. *Science* **1992**, *255*, 848−850.

(5) Garrido Montalban, A.; Meunier, H. G.; Ostler, R. B.; Barrett, A. G. M.; Hoffman, B. M.; Rumbles, G. *J. Phys. Chem. A* **1999**, *103*, 4352−4358.

(6) (a) Dadon, Z.; Samiappan, M.; Safranchik, E. Y.; Ashkenasy, G. *Chem.—Eur. J.* **2010**, *16*, 12096−12099. (b) Samiappan, M.; Dadon, Z.; Ashkenasy, G. *Chem. Commun.* **2011**, *47*, 710−712. (c) Dadon, Z.; Samiappan, M.; Wagner, N.; Ashkenasy, G. *Chem. Commun.* **2012**, *48*, 1419−1421.

(7) (a) Kottani, R. R.; Majjigapu, J. R. R.; Kurchan, A. N.; Majjigapu, K.; Gustafson, T. P.; Kutateladze, A. G. *J. Am. Chem. Soc.* **2006**, *128*, 14794−14795. (b) Gustafson, T. P.; Metzel, G. A.; Kutateladze, A. G. *Org. Biomol. Chem.* **2011**, *9*, 4752−4755. (c) Gustafson, T. P.; Metzel, G. A.; Kutateladze, A. G. *Photochem. Photobiol. Sci.* **2012**, *11*, 564−577.

(8) Sella, E.; Lubelski, A.; Klafter, J.; Shabat, D. *J. Am. Chem. Soc.* **2010**, *132*, 3945−3952.

(9) Vignoni, M.; Cabrerizo, F. M.; Lorente, C.; Claparols, C.; Oliveros, E.; Thomas, A. *Org. Biomol. Chem.* **2010**, *8*, 800−810.

(10) Dutta, S.; Mokhir, A. *Chem. Commun.* **2011**, *47*, 1243−1245.

(11) Thomas, S. W., III; Joly, G. D.; Swager, T. M. *Chem. Rev.* **2007**, *107*, 1339−1386.

(12) Raymo, F. M. *Phys. Chem. Chem. Phys.* **2013**, *15*, 14840−14850.

(13) Raymo, F. M. *ISRN Phys. Chem.* **2012**, 619251−1−15.

(14) Raymo, F. M. *J. Phys. Chem. Lett.* **2012**, *3*, 2379−2385.

(15) Hyndman, H. L.; Monroe, B. M.; Hammond, G. S. *J. Am. Chem. Soc.* **1969**, *91*, 2852−2859.

(16) (a) Saltiel, J.; Townsend, D. E.; Skyes, A. *J. Am. Chem. Soc.* **1973**, *95*, 5968−5973. (b) Saltiel, J.; Zhang, Y. X.; Sears, D. F. *J. Am. Chem. Soc.* **1997**, *46*, 11202−11210. (c) Saltiel, J.; Wang, S.; Ko, D.-H.; Groming, D. A. *J. Phys. Chem. A* **1998**, *102*, 5383−5392. (d) Saltiel, J.; Crowder, J. M.; Wang, S. J. *J. Am. Chem. Soc.* **1999**, *121*, 895−902. (e) Saltiel, J.; Dmitrenko, O.; Reischl, W.; Bach, R. D. *J. Phys. Chem. A* **2001**, *105*, 3934−3939. (f) Saltiel, J.; Dmitrenko, O.; Pillai, Z. S.; Klima, R.; Wang, S.; Wharton, T.; Huang, Z.-N.; van de Burgt, L. J.; Arranz, J. *Photochem. Photobiol. Sci.* **2008**, *7*, 566−577.

(17) (a) Lechtken, P.; Yekta, A.; Turro, N. J. *J. Am. Chem. Soc.* **1973**, *95*, 3027−3028. (b) Turro, N. J.; Schore, N. E.; Steinmet, H. C.; Yekta, A. *J. Am. Chem. Soc.* **1974**, *96*, 1936−1938. (c) Renner, C. A.; Katz, T. J.; Pouliquen, J.; Turro, N. J.; Waddell, W. H. *J. Am. Chem. Soc.* **1975**, *97*, 2568−2570. (d) Turro, N. J.; Waddell, W. H. *Tetrahedron Lett.* **1975**, 2069−2072. (e) Lechtken, P.; Yekta, A.; Shore, N. E.; Steinmetzer, H. C.; Waddell, W. H.; Turro, N. J. *Z. Phys. Chem.* **1976**, *101*, 79−90. (f) Turro, N. J.; Ramamurthy, V.; Katz, T. J. *Nouv. J. Chim.* **1977**, *1*, 363−365.

(18) (a) Okamoto, H.; Arai, T.; Sakuragi, H.; Tokumaru, K.; Kawanishi, Y. *Bull. Chem. Soc. Jpn.* **1991**, *64*, 216−220. (b) Karatsu, T.; Hiresaki, T.; Arai, T.; Sakuragi, H.; Tokumaru, K.; Wirz, J. *Bull. Chem. Soc. Jpn.* **1991**, *64*, 3355−3362. (c) Lednev, I. K.; Alfimov, M. V.; Kuriyama, Y.; Arai, T.; Sakuragi, H.; Tokumaru, K. *J. Photochem. Photobiol.* **1992**, *63*, 201−209. (d) Arai, T.; Furuya, Y.; Furuuchi, H.; Tokumaru, K. *Chem. Phys. Lett.* **1993**, *212*, 597−603. (e) Karatsu, T.; Tsuchiya, M.; Arai, T.; Sakuragi, H.; Tokumaru, K. *Bull. Chem. Soc. Jpn.* **1994**, *67*, 3030−3039. (f) Arai, T.; Takahashi, O.; Asano, T.; Tokumaru, K. *Chem. Lett.* **1994**, 205−208. (g) Tokumaru, K.; Arai, T. *Bull. Chem. Soc. Jpn.* **1995**, *68*, 1065−1087.

(19) (a) Merkel, P. B.; Roh, Y.; Dinnocenzo, J. P.; Robello, D. R.; Farid, S. *J. Phys. Chem. A* **2007**, *111*, 1188−1199. (b) Ferrar, L.; Mis, M.; Dinnocenzo, J. P.; Farid, S.; Merkel, P. B.; Robello, D. R. *J. Org. Chem.* **2008**, *73*, 5683−5692.

(20) (a) Kuzmanich, G.; Natarajan, A.; Chin, K.; Veerman, M.; Mortko, C.; Garcia-Garibay, M. A. *J. Am. Chem. Soc.* **2008**, *130*, 1140−1141. (b) Kuzmanich, G.; Gard, M.; Garcia-Garibay, M. A. *J. Am. Chem. Soc.* **2009**, *131*, 11606−11614. (c) Nielsen, A.; Kuzmanich, G.; Garcia-Garibay, M. A. *J. Phys. Chem. A* **2014**, *118*, 1858−1863.

(21) Alvarez-Puebla, R. A.; Liz-Marzán, L. M.; García de Abajo, F. J. *J. Phys. Chem. Lett.* **2010**, *1*, 2428−2434.

(22) Scaiano, J. C.; Stamplecoskie, K. *J. Phys. Chem. Lett.* **2013**, *4*, 1177−1188.

(23) Nabika, H.; Takase, M.; Nagasawa, F.; Murakoshi, K. *J. Phys. Chem. Lett.* **2010**, *1*, 2470−2487.

(24) Strating, J.; Zwanenburg, B.; Wagenaar, A.; Udding, A. C. *Tetrahedron Lett.* **1969**, *10*, 125−128.

(25) Mondal, R.; Shah, B. K.; Neckers, D. C. *J. Am. Chem. Soc.* **2006**, *128*, 9612−9613.

(26) (a) Mondal, R.; Okhrimenko, A. N.; Shah, B. K.; Neckers, D. C. *J. Phys. Chem. B* **2008**, *112*, 11−15. (b) Bettinger, H. F.; Mondal, R.; Krasowska, M.; Neckers, D. C. *J. Org. Chem.* **2013**, *78*, 1851−1857.

(27) Suzuki, M.; Aotake, T.; Yamaguchi, Y.; Noguchi, N.; Nakano, H.; Nakayama, K.; Yamada, H. *J. Photochem. Photobiol., C* **2014**, *18*, 50−70.

(28) (a) Aotake, T.; Tanimoto, H.; Hotta, H.; Kuzuhara, D.; Okujima, T.; Uno, H.; Yamada, H. *Chem. Commun.* **2013**, *49*, 3661−3663. (b) Aotake, T.; Yamashita, Y.; Okujima, T.; Shirasawa, N.; Jo, Y.; Fujimori, S.; Uno, H.; Ono, N.; Yamada, H. *Tetrahedron Lett.* **2013**, *54*, 1790−1793.

(29) Peng, P.; Wang, C. M.; Shi, Z.; Johns, V. K.; Ma, L. Y.; Oyer, J.; Copik, A.; Igarashi, R.; Liao, Y. *Org. Biomol. Chem.* **2013**, *11*, 6671−6674.

(30) (a) Mondal, R.; Adhikari, R. M.; Shah, B. K.; Neckers, D. C. *Org. Lett.* **2007**, *9*, 2505−2508. (b) Zhao, Y.; Mondal, R.; Neckers, D. C. *J. Org. Chem.* **2008**, *73*, 5506−5513. (c) Mondal, R.; Tönshoff, C.; Khon, D.; Neckers, D. C.; Bettinger, H. F. *J. Am. Chem. Soc.* **2009**, *131*, 14281−14289.

(31) Tönshoff, C.; Bettinger, H. F. *Angew. Chem., Int. Ed.* **2010**, *48*, 4125−4128.

(32) Wright, M. W.; Welker, M. E. *J. Org. Chem.* **1996**, *61*, 133−141.

(33) Only one of the two anthracene chromophores absorbs at 390 nm. Instead, both compounds have similar molar absorption coefficients at 350 nm. As a result, the behavior of the two diketones under illumination was compared using the latter wavelength (Figure 6a,b). Under these conditions, the spectral changes observed for **2** are similar to those detected with an illumination wavelength of 390 nm (Figure 5).

(34) The average distance between the many molecules immobilized within the rigid polymer matrix is 32 Å at this particular dopant loading. This distance value was estimated from the molar concentration of the reactant (**1** or **2**) in PBMA. The latter parameter was determined from the corresponding absorbance at 462 nm (Figure 4a,b), the molar absorption coefficient determined in MeCN (Figure S5a,b (SI)) and the film thickness (2.5 μm) measured with a surface profilometer.

(35) A literature precedent (ref 20c) demonstrates that Dexter energy transfer governs the cascade responsible for quantum amplification in the photoinduced decarbonylation of a diarylcyclopropanone. In principle, such a mechanism could also contribute to the ability of **4** to sensitize its own formation from **2**. Considering the exponential dependence of Dexter energy transfer on the donor−acceptor separation, however, its efficiency should be negligible at the relatively long distance (32 Å) between **2** and **4** ensured by the selected experimental conditions (ref 34).

(36) In principle, **2** can reabsorb part of the photons emitted by **4** and undergo decarbonylation as a result. However, the contribution of this radiative process, if at all occurring, to the sensitized formation of **4** is most likely negligible under the conditions selected for these experiments. Indeed, the absorbance of the $n \rightarrow \pi^*$ band of **2** is less than 0.01 in all instances and such small values ensure insignificant reabsorption.

(37) The mathematical model employed to fit the photokinetic profiles is reported in the Supporting Information.

(38) Lakowicz, J. R.; Shen, Y.; Auria, S. D.; Malicka, J.; Fang, J.; Gryczynski, Z.; Gryczynski, I. *Anal. Biochem.* **2002**, *301*, 261−277.

(39) Goichi, M.; Segawa, K.; Suzuki, S.; Toyota, S. *Synthesis* **2005**, 2116−2118.

(40) Thapaliya, E. R.; Captain, B.; Raymo, F. M. *J. Org. Chem.* **2014**, *79*, 3973−3981.

(41) Scaiano, J. C., Ed.; *Handbook of Organic Photochemistry*; CRC Press: Boca Raton, FL, 1989.

(42) *Apex2 Version 2.2−0 and SAINT+ Version 7.46A*; Bruker Analytical X-ray System, Inc.: Madison, WI, 2007.

(43) (a) Sheldrick, G. M. *SHELXTL Version 6.1*; Bruker Analytical X-ray Systems, Inc.: Madison, WI, 2000. (b) Sheldrick, G. M. *Acta Crystallogr.* **2008**, *A64*, 112−122.